

# Planar Hall effect in the Dirac semimetal PdTe<sub>2</sub>

Sheng Xu,\* Huan Wang,\* Xiao-Yan Wang, Yuan Su, Peng Cheng, and Tian-Long Xia<sup>†</sup>

*Department of Physics, Renmin University of China, Beijing 100872, P. R. China and  
Beijing Key Laboratory of Opto-electronic Functional Materials & Micro-nano Devices,  
Renmin University of China, Beijing 100872, P. R. China*

(Dated: November 19, 2018)

We report the synthesis and magneto-transport measurements on the single crystal of Dirac semimetal PdTe<sub>2</sub>. The de Haas-van Alphen oscillations with multiple frequencies have been clearly observed, from which the small effective masses and nontrivial Berry phase are extracted, implying the possible existence of the Dirac fermions in PdTe<sub>2</sub>. The planar Hall effect and anisotropic longitudinal resistivity originating from the chiral anomaly and nontrivial Berry phase are observed, providing strong evidence for the nontrivial properties in PdTe<sub>2</sub>. With the increase of temperature up to 150 K, planar Hall effect still remains. The possible origin of mismatch between experimental results and theoretical predictions is also discussed.

## I. INTRODUCTION

Topological Dirac/Weyl semimetals have attracted extensive attention in condensed matter physics community because of their novel properties<sup>1-9</sup>. In the Dirac semimetals, the fourfold degenerate band crossings in the vicinity of the Fermi level are known as Dirac points<sup>10</sup>. As the inversion symmetry or time reversal symmetry breaks, Dirac point degenerates into Weyl points with opposite chirality<sup>11</sup>. Interestingly, the parallel magnetic and electric field pumps electrons between Weyl nodes with opposite chirality, which leads to a chiral current that contributes to the negative magnetoresistance (NMR)<sup>12-14</sup>. The observation of the NMR has been regarded as a routine method to study Dirac/Weyl fermions in transport measurements. However, the NMR may also be contributed by other mechanisms<sup>15-21</sup>, and sometimes it is hard to clearly observe the chiral anomaly induced NMR in some topological semimetals with the coexisting positive orbital MR. The nontrivial Berry phase extracted from the quantum oscillations provides another evidence for the identification of the topological characteristics. However, it is difficult to extract the Berry phase from those materials with complex band structures or the materials without observable quantum oscillations.

It is worth noting that planar Hall effect (PHE), another characteristic induced by the chiral anomaly and nontrivial Berry phase, is predicted as a proof of the existence of Weyl fermions in the topological semimetals when the applied magnetic and electric fields are coplanar<sup>22,23</sup>, which is already observed in GdPtBi<sup>24</sup>/DyPdBi<sup>25</sup>, VAl<sub>3</sub><sup>26</sup>, Mo/WTe<sub>2</sub><sup>27-29</sup>, Cd<sub>3</sub>As<sub>2</sub><sup>30,31</sup> and ZrTe<sub>5- $\delta$</sub> <sup>32</sup>, TaP<sup>33</sup>. On the other hand, the PHE with a smaller value is also observed in some topological trivial ferromagnetic metals, which originates from the interplay of magnetic order and spin-orbit interaction<sup>34</sup>. Thus, PHE is believed as a direct evidence in magneto-transport studies to identify the nontrivial topological property in nonmagnetic materials, especially for those candidates in which band structures are complex, oscillations are absent or the NMR is difficult to observe.

The transitional metal dichalcogenide PdTe<sub>2</sub> is believed to be type-II Dirac semimetal as PtTe<sub>2</sub><sup>35-39</sup>. In this paper, we report the magneto-transport measurements of nonmagnetic PdTe<sub>2</sub> with the de Haas-van Alphen (dHvA) oscillations

observed, from the analysis of which the multiple frequencies, effective masses and nontrivial Berry phase are extracted. The PHE and anisotropic longitudinal resistivity are observed, which provides a strong evidence for the existence of topological nontrivial properties in PdTe<sub>2</sub>.

The single crystals of PdTe<sub>2</sub> were grown by melting the mixture of Pd and Te powder with a ratio 1:2.2 in a sealed evacuated quartz tube at 800°C for 2 days, then slowly cooling down in 7 days to 500°C, and remaining for 7 days before turning off the furnace. The pattern of XRD was collected from a Bruker D8 Advance x-ray diffractometer using Cu K $\alpha$  radiation. The magneto-transport measurements were performed on a Quantum Design physical property measurement system (QD PPMS).

## II. RESULTS AND DISCUSSION

The x-ray diffraction (XRD) pattern of single crystal with strongly (00l) peaks is shown in Fig.1 (a), which indicates that the surface of the crystal is the ab plane. The inset of Fig.1 (a) shows a typical picture of grown PdTe<sub>2</sub> crystal with metallic luster. Clear dHvA oscillations are observed in PdTe<sub>2</sub> crystals at the temperature range 2 K - 30 K with the magnetic field parallel to the c-axis (B//c) as shown in Fig.1 (b). With the temperature increasing, the oscillations gradually weaken. After subtracting a smoothing background, the oscillatory amplitudes of magnetization against 1/B were plotted in Fig.1 (c). The extracted frequencies from the fast Fourier transform (FFT) analysis are shown in Fig.1 (d). The oscillations can be well described by the Lifshitz-Kosevich (LK) formula<sup>40</sup>,

$$\Delta M \propto -B^{1/2} \frac{\lambda T}{\sinh(\lambda T)} e^{-\lambda T_D} \sin\left[2\pi\left(\frac{F}{B} - \frac{1}{2} + \beta + \delta\right)\right] \quad (1)$$

where  $\lambda = (2\pi^2 k_B m^*)/(\hbar e B)$ ,  $T_D$  is the Dingle temperature and  $\beta = \Phi_B/2\pi$  ( $\Phi_B$  is the Berry phase). The phase shift  $\delta$  is determined by the dimensionality,  $\delta = 0$  and  $\delta = \pm 1/8$  for 2D and 3D system, respectively. The thermal factor  $R_T = (\lambda T)/\sinh(\lambda T)$  in LK formula is employed to fit the temperature dependence of the oscillatory amplitude (Fig.1 (e)).

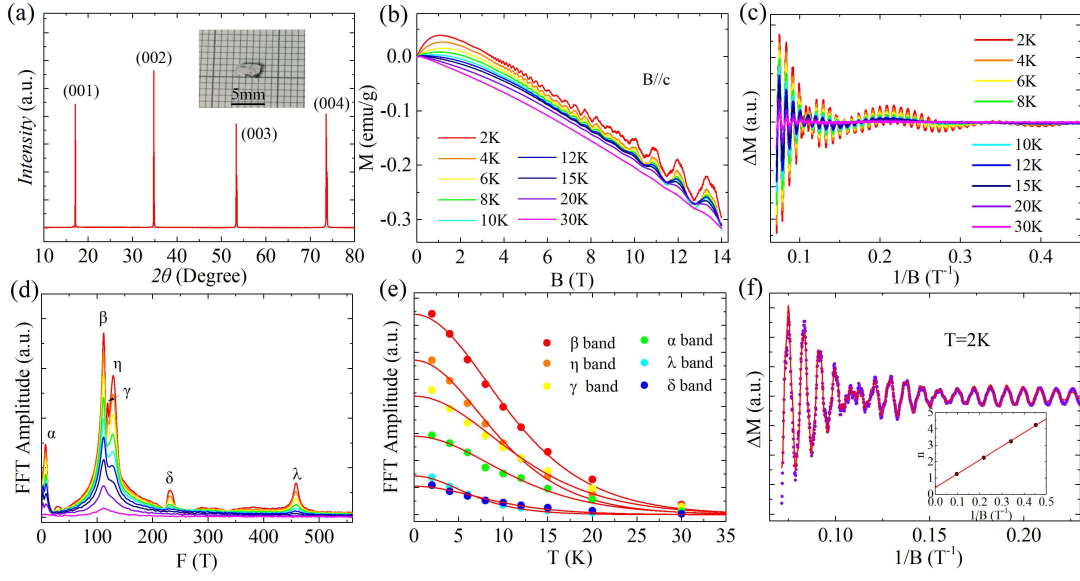


FIG. 1: (a) XRD of the PdTe<sub>2</sub> single crystal. Inset shows the picture of a grown crystal. (b) The dHvA oscillations of PdTe<sub>2</sub> at various temperatures. (c) The amplitude of dHvA oscillations plotted as a function of  $1/B$ . (d) FFT spectra of the oscillations between 5 K and 30 K. (e) The temperature dependence of relative FFT amplitudes of each frequency and the fitting results by  $R_T$ . (f) The LK formula fitting of the dHvA oscillations excluding the  $\alpha$  band. The inset shows the LL index fan diagram for  $\alpha$  band.

The effective masses around  $0.04\text{-}0.08m_e$  obtained from the fitting are listed in Table I. The Berry phase  $\Phi_B = 2\pi\beta$  can be extracted from the fitting of the LK formula or the analysis of Landau level (LL) index fan diagram. We adopt the latter method to extract the Berry phase of  $\alpha$  band, and the corresponding LL index fan diagram is shown in Fig.1 (f). The Landau index of the dHvA oscillations maximum should be  $n+1/4$ <sup>41</sup>, and the LL index fan diagram gives an intercept of 0.43 which is consistent with previous reports<sup>37,38</sup>. Thus, the Berry phase of  $\alpha$  band is obtained to be  $2.11\pi$  for  $\delta = -1/8$  or  $1.61\pi$  for  $\delta = 1/8$ , respectively. Both of them are close to  $2\pi$ , which indicates the topological trivial character of  $\alpha$  band. After filtering the frequency of  $\alpha$  band, we obtained the high frequency oscillations as shown in Fig.1 (f) (violet dots). The Berry phases are extracted from the fitting of the multiband LK formula (red line), and the corresponding values are listed in Table I. Several of the Berry phases are close to the nontrivial value  $\pi$  indicating the possible existence of Dirac fermions in PdTe<sub>2</sub>.

The PHE is also examined to further study whether the topological nontrivial states exist in PdTe<sub>2</sub>. The planar Hall resistivity ( $\rho_{xy}^{PHE}$ ) and anisotropic longitudinal resistivity ( $\rho_{xx}$ ) measurements with the coplanar magnetic and electric field are reported in details. As the theory predicts, the angular dependence of PHE and anisotropic longitudinal resistivity in the Dirac/Weyl semimetals can be described as,

$$\rho_{xy}^{PHE} = -\Delta\rho^{chiral} \sin\theta \cos\theta \quad (2)$$

$$\rho_{xx} = \rho_{\perp} - \Delta\rho^{chiral} \cos^2\theta \quad (3)$$

where  $\rho_{xy}^{PHE}$  is the planar Hall resistivity, and  $\Delta\rho^{chiral} = \rho_{\perp} - \rho_{\parallel}$  is the chiral anomaly induced resistivity component

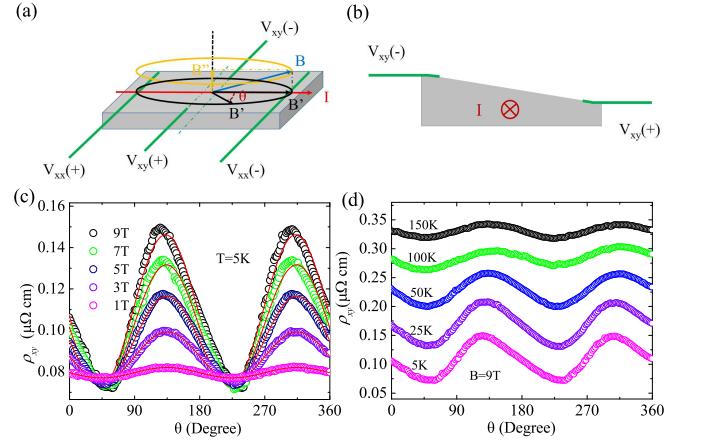


FIG. 2: (a) Schematic diagram for the planar Hall resistivity measurements and the misalignments geometry. (b) Lateral view of the schematic diagram in (a). (c) The angular dependence of  $\rho_{xy}$  under various magnetic fields at 5 K. (d) The planar Hall resistivity  $\rho_{xy}$  as a function of angle at different temperatures ( $B=9$  T).

when the current and the magnetic field are coplanar ( $\rho_{\perp}$  or  $\rho_{\parallel}$  represents the resistivity with the magnetic field perpendicular or parallel to the current, respectively).  $\theta$  is defined as the angle between the current and magnetic field direction.  $\rho_{xx}$  corresponds to the angle-dependent longitudinal resistivity. The results can not be well described with the Eqs. (2) and (3). Considering the actual difficulties in the measurements, the disagreement is attributed to three types of misalignments. The first one is that the current and the magnetic field  $B$  (cyan line in Fig.2 (a)) may not be completely coplanar due to the tilt of the sample. Hence, an additional magnetic component

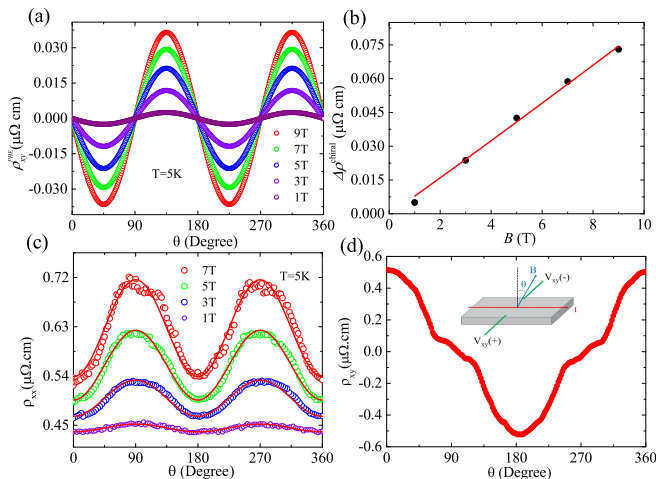


FIG. 3: (a) The extracted intrinsic planar Hall resistivity  $\rho_{xy}^{PHE}$  versus angle  $\theta$  under different magnetic fields ( $T=5$  K). (b) The extracted parameter  $a$  varies linearly with magnetic field at  $T=5$  K. (c) The anisotropic longitudinal resistivity under different magnetic fields at 5 K. (d) The angular dependence of the normal Hall resistivity at 10 K. The inset shows the schematic diagram for the normal Hall resistivity measurement.

$B''$  (yellow line in Fig.2 (a)) normal to the sample surface is induced and leads to an unexpected normal Hall resistance. The parallel component  $B'$  rotates in the sample plane with the angle  $\theta$  from the direction of the current, as illustrated in Fig.2 (a). It is fortunate that the normal Hall resistivity complies with an odd function versus magnetic field while planar Hall resistivity is not (even function). The influence of the normal Hall resistance can be easily subtracted by taking an average of the data obtained under the positive and negative magnetic field. The second type of misalignment originates from the asymmetrical Hall contacts which introduce an extra longitudinal resistivity and can be described as  $b\cos^2\theta$ . The last one is attributed to the non-uniform thickness of the sample, which leads to a constant Hall resistivity. To demonstrate the analysis clearly, a schematic diagram is presented to show the planar Hall resistivity measurement and the misalignments as displayed in Fig.2 (a). The lateral view exhibiting non-uniform thickness of the sample is also shown in Fig.2 (b). Thus, Eq. (2) is modified as,

$$\rho_{xy} = -a\sin\theta\cos\theta + b\cos^2\theta + c \quad (4)$$

the first part is the intrinsic PHE term  $\rho_{xy}^{PHE}$  induced by the chiral anomaly and the nontrivial Berry phase. The second and third are modified terms corresponding to the latter two kinds of misalignments.

Figure 2(c) shows the angular dependence of  $\rho_{xy}$  under various magnetic field at 5 K, which have eliminated the extra normal Hall resistivity by taking the average of the values obtained under positive and negative fields. The observed  $\rho_{xy}$  exhibits the valley at  $\pi/4$  and the peak at  $3\pi/4$  with the period of  $\pi$ , which is well fitted by the Eq. (4). The fitting results

are demonstrated as the red curves in Fig.2 (c). Even though

TABLE I: Parameters derived from the dHvA oscillations.  $F$ , oscillation frequency;  $m^*$ , effective mass;  $\Phi_B = 2\pi\beta$ , Berry phase.

	$F$ (T)	$m^*/m_e$	$\Phi_B = 2\pi\beta$ ( $\delta = 1/8$ )	$\Phi_B = 2\pi\beta$ ( $\delta = -1/8$ )	$\Phi_B = 2\pi\beta$ ( $\delta = 0$ )
$\alpha$	7.4	0.05	$2.11\pi$	$1.61\pi$	/
$\beta$	112.0	0.05	$0.01\pi$	$1.51\pi$	$1.76\pi$
$\gamma$	119.3	0.04	$1.11\pi$	$0.61\pi$	$0.86\pi$
$\eta$	129.3	0.05	$1.30\pi$	$0.80\pi$	$1.05\pi$
$\delta$	230.9	0.08	$0.54\pi$	$0.04\pi$	$0.29\pi$
$\lambda$	458.6	0.06	$1.84\pi$	$1.33\pi$	$1.59\pi$

the amplitude of the PHE decreases with the increasing temperature, the PHE is still observed up to 150 K.

The intrinsic PHE extracted from the fitting by Eq. (4) is plotted in Fig.3 (a). The amplitudes of PHE at different field are displayed in Fig.3 (b), which shows a  $B$  dependence. In addition, we plotted the anisotropic longitudinal resistivity under different magnetic field at 5 K as shown in Fig.3 (c). The observed  $\rho_{xx}$  demonstrates the period of  $\pi$  with maximum at  $\pi/2$  and  $3\pi/2$  when the magnetic field is applied normal to the current. The curves in red shown in Fig.3 (c) represent the fitting by Eq. (3), which coincide well with the experimental results. To clarify the difference from the PHE, the normal Hall measurement is applied. Fig.3 (d) shows the angular dependence of the normal Hall resistivity at 10 K demonstrating the period of  $2\pi$ , twice as much as that in PHE.

### III. SUMMARY

In conclusion, we have grown high quality single crystals of PdTe<sub>2</sub> and investigated the magneto-transport properties. The dHvA oscillations with multiple frequencies have been observed. According to the analysis of the oscillations, we obtained small effective masses and nontrivial Berry phase, which suggest the possible existence of Dirac/Weyl fermions. Also, a clear signal of PHE and the anisotropic longitudinal resistivity are observed, which can be regarded as the result of the chiral anomaly and nontrivial Berry phase. Besides, taking the noncoplanar magnetic field with the sample, non-uniform sample thickness and asymmetrical Hall contacts into consideration, the modified model agrees well with the data obtained. Thus, the nontrivial Berry phase extracted from the dHvA oscillations indicates the topological nontrivial characteristic of PdTe<sub>2</sub>, while the PHE provides the further evidence.

### IV. ACKNOWLEDGMENTS

This work is supported by the National Natural Science Foundation of China (No.11574391, No.11874422), the Fundamental Research Funds for the Central Universities, and the Research Funds of Renmin University of China (No.18XNLG14).

\* These authors contributed equally to this paper

† Electronic address: tlxia@ruc.edu.cn

- <sup>1</sup> Z. Liu, B. Zhou, Y. Zhang, Z. Wang, H. Weng, D. Prabhakaran, S.-K. Mo, Z. Shen, Z. Fang, X. Dai, *et al.*, *Science* **343**, 864 (2014).
- <sup>2</sup> J. Xiong, S. K. Kushwaha, T. Liang, J. W. Krizan, M. Hirschberger, W. Wang, R. Cava, and N. Ong, *Science* **350**, 413 (2015).
- <sup>3</sup> M. Neupane, S.-Y. Xu, R. Sankar, N. Alidoust, G. Bian, C. Liu, I. Belopolski, T.-R. Chang, H.-T. Jeng, H. Lin, *et al.*, *Nat. Commun.* **5**, 3786 (2014).
- <sup>4</sup> Z. Liu, J. Jiang, B. Zhou, Z. Wang, Y. Zhang, H. Weng, D. Prabhakaran, S. Mo, H. Peng, P. Dudin, *et al.*, *Nat. Mater.* **13**, 677 (2014).
- <sup>5</sup> S. Borisenko, Q. Gibson, D. Evtushinsky, V. Zabolotnyy, B. Büchner, and R. J. Cava, *Phys. Rev. Lett.* **113**, 027603 (2014).
- <sup>6</sup> T. Liang, Q. Gibson, M. N. Ali, M. Liu, R. Cava, and N. Ong, *Nat. Mater.* **14**, 280 (2015).
- <sup>7</sup> C.-Z. Li, L.-X. Wang, H. Liu, J. Wang, Z.-M. Liao, and D.-P. Yu, *Nat. Commun.* **6**, 10137 (2015).
- <sup>8</sup> H. Li, H. He, H. Lu, H. Zhang, H. Liu, R. Ma, Z. Fan, S. Shen, and J. Wang, *Nat. Commun.* **7**, 10301 (2015).
- <sup>9</sup> H. Weng, C. Fang, Z. Fang, B. A. Bernevig, and X. Dai, *Phys. Rev. X* **5**, 011029 (2015).
- <sup>10</sup> T. Wehling, A. M. Black-Schaffer, and A. V. Balatsky, *Adv. Phys.* **63**, 1 (2014).
- <sup>11</sup> X. Wan, A. M. Turner, A. Vishwanath, and S. Y. Savrasov, *Phys. Rev. B* **83**, 205101 (2011).
- <sup>12</sup> X. Huang, L. Zhao, Y. Long, P. Wang, D. Chen, Z. Yang, H. Liang, M. Xue, H. Weng, Z. Fang, *et al.*, *Phys. Rev. X* **5**, 031023 (2015).
- <sup>13</sup> C.-L. Zhang, S.-Y. Xu, I. Belopolski, Z. Yuan, Z. Lin, B. Tong, G. Bian, N. Alidoust, C.-C. Lee, S.-M. Huang, *et al.*, *Nat. Commun.* **7**, 10735 (2016).
- <sup>14</sup> D. Son and B. Spivak, *Phys. Rev. B* **88**, 104412 (2013).
- <sup>15</sup> L. Ritchie, G. Xiao, Y. Ji, T. Chen, C. Chien, M. Zhang, J. Chen, Z. Liu, G. Wu, and X. Zhang, *Phys. Rev. B* **68**, 104430 (2003).
- <sup>16</sup> B. Fauqué, D. LeBoeuf, B. Vignolle, M. Nardone, C. Proust, and K. Behnia, *Phys. Rev. Lett.* **110**, 266601 (2013).
- <sup>17</sup> A. B. Pippard, *Magnetoresistance in metals*, Vol. 2 (Cambridge University Press, 1989).
- <sup>18</sup> J. Hu, T. Rosenbaum, and J. Betts, *Phys. Rev. Lett.* **95**, 186603 (2005).
- <sup>19</sup> N. Kikugawa, P. Goswami, A. Kiswandhi, E. Choi, D. Graf, R. Baumbach, J. Brooks, K. Sugii, Y. Iida, M. Nishio, *et al.*, *Nat. Commun.* **7**, 10903 (2016).
- <sup>20</sup> T. Osada, *J. Phys. Soc. Jpn.* **77**, 084711 (2008).
- <sup>21</sup> N. Tajima, S. Sugawara, R. Kato, Y. Nishio, and K. Kajita, *Phys. Rev. Lett.* **102**, 176403 (2009).
- <sup>22</sup> A. Burkov, *Phys. Rev. B* **96**, 041110 (2017).
- <sup>23</sup> S. Nandy, G. Sharma, A. Taraphder, and S. Tewari, *Phys. Rev. Lett.* **119**, 176804 (2017).
- <sup>24</sup> N. Kumar, S. N. Guin, C. Felser, and C. Shekhar, *Phys. Rev. B* **98**, 041103 (2018).
- <sup>25</sup> O. Pavlosiuk, D. Kaczorowski, and P. Wisniewski, arXiv preprint arXiv:1808.06856 (2018).
- <sup>26</sup> R. Singha, S. Roy, A. Pariari, B. Satpati, and P. Mandal, *Phys. Rev. B* **98**, 081103R (2018).
- <sup>27</sup> D. Liang, Y. Wang, W. Zhen, J. Yang, S. Weng, X. Yan, Y. Han, W. Tong, L. Pi, W. Zhu, *et al.*, arXiv preprint arXiv:1809.01290 (2018).
- <sup>28</sup> F. Chen, X. Luo, J. Yan, Y. Sun, H. Lv, W. Lu, C. Xi, P. Tong, Z. Sheng, X. Zhu, *et al.*, *Phys. Rev. B* **98**, 041114R (2018).
- <sup>29</sup> Y. Wang, J. Gong, D. Liang, M. Ge, J. Wang, W. Zhu, and C. Zhang, arXiv preprint arXiv:1801.05929 (2018).
- <sup>30</sup> H. Li, H.-W. Wang, H. He, J. Wang, and S.-Q. Shen, *Phys. Rev. B* **97**, 201110R (2018).
- <sup>31</sup> M. Wu, G. Zheng, W. Chu, Y. Liu, W. Gao, H. Zhang, J. Lu, Y. Han, J. Zhou, W. Ning, *et al.*, *Phys. Rev. B* **98**, 161110R (2018).
- <sup>32</sup> P. Li, C. Zhang, J. Zhang, Y. Wen, and X. Zhang, *Phys. Rev. B* **98**, 121108R (2018).
- <sup>33</sup> J. Yang, W. Zhen, D. Liang, Y. Wang, X. Yan, S. Weng, J. Wang, W. Tong, L. Pi, W. Zhu, *et al.*, arXiv preprint arXiv:1807.06229 (2018).
- <sup>34</sup> A. Nazmul, H. Lin, S. Tran, S. Ohya, and M. Tanaka, *Phys. Rev. B* **77**, 155203 (2008).
- <sup>35</sup> Y. Wang, J. Zhang, W. Zhu, Y. Zou, C. Xi, L. Ma, T. Han, J. Yang, J. Wang, J. Xu, *et al.*, *Sci Rep* **6**, 31554 (2016).
- <sup>36</sup> H. J. Noh, J. Jeong, E. J. Cho, K. Kim, B. I. Min, and B. G. Park, *Phys. Rev. Lett.* **119**, 016401 (2017).
- <sup>37</sup> F. Fei, X. Bo, R. Wang, B. Wu, J. Jiang, D. Fu, M. Gao, H. Zheng, Y. Chen, X. Wang, *et al.*, *Phys. Rev. B* **96**, 041201 (2017).
- <sup>38</sup> W. Zheng, R. Schönemann, N. Aryal, Q. Zhou, D. Rhodes, Y.-C. Chiu, K.-W. Chen, E. Kampert, T. Förster, T. Martin, *et al.*, *Phys. Rev. B* **97**, 235154 (2018).
- <sup>39</sup> M. Yan, H. Huang, K. Zhang, E. Wang, W. Yao, K. Deng, G. Wan, H. Zhang, M. Arita, H. Yang, *et al.*, *Nat. Commun.* **8**, 257 (2017).
- <sup>40</sup> D. Shoenberg, *Magnetic oscillations in metals* (Cambridge University Press, 2009).
- <sup>41</sup> J. Hu, Z. Tang, J. Liu, X. Liu, Y. Zhu, D. Graf, K. Myhro, S. Tran, C. N. Lau, J. Wei, *et al.*, *Phys. Rev. Lett.* **117**, 016602 (2016).